AIP | Journal of Applied Physics

Experimental and theoretical demonstration of acoustic Bloch oscillations in porous silicon structures

Z. Lazcano, J. Arriaga, and G. N. Aliev

Citation: Journal of Applied Physics **115**, 154505 (2014); doi: 10.1063/1.4871535
View online: http://dx.doi.org/10.1063/1.4871535
View Table of Contents: http://scitation.aip.org/content/aip/journal/jap/115/15?ver=pdfcov
Published by the AIP Publishing

Experimental and theoretical demonstration of acoustic Bloch oscillations in porous silicon structures

Z. Lazcano,[1] J. Arriaga,[1,a)] and G. N. Aliev[2]
[1]*Instituto de Física, Benemérita Universidad Autónoma de Puebla, 18 Sur y San Claudio, Edif. 110-A, Ciudad Universitaria, 72570 Puebla, Mexico*
[2]*Department of Physics, University of Bath, Claverton Down, Bath BA2 7AY, United Kingdom*

(Received 25 November 2013; accepted 4 April 2014; published online 16 April 2014)

We report the theoretical calculations and the experimental demonstration of acoustic Bloch oscillations and Wannier-Stark ladders in linear tilted multilayer structures based on porous silicon. The considered structures consist of layers with constant porosity alternated by layers with a linear gradient in the parameter $\eta = 1/v_L^2$ along the growth direction in order to tilt the acoustic band gap. The purpose of this gradient is to mimic the tilted electronic miniband structure of a superlattice semiconductor under an external electric field. In this way, acoustic Wannier-Stark ladders of equidistant modes are formed and they were experimentally confirmed in the transmission spectrum around 1.2 GHz. Their frequency separation defines the period of the acoustic Bloch oscillations. We fabricated three different structures with the same thicknesses but different values in the η parameter to observe the effect on the period of the Bloch oscillations. We measured the acoustic transmission spectra in the frequency domain, and by using the Fourier transform, we obtained the transmission in the time domain. The transmission spectra of the fabricated samples show acoustic Bloch oscillations with periods of 27, 24, and 19 ns. The experimental results are in good agreement with the transfer matrix calculations. The observed phenomenon is the acoustic counterpart of the well known electronic Bloch oscillations. © *2014 AIP Publishing LLC*. [http://dx.doi.org/10.1063/1.4871535]

I. INTRODUCTION

In 1928, it was shown, by using a semi-classical analysis, that the dynamic of an electronic wave packet in a crystal under the influence of a uniform external electric field displays a completely non-trivial behavior: It undergoes an oscillatory movement known as Bloch oscillations (BOs).[1] The frequency counterpart of BO are the Wannier-Stark ladders (WSLs), a set of equally spaced frequency resonances with the nearest-neighbor level spacing being proportional to the intensity of the external field.[2] The existence of these WSL was first confirmed by numerical simulations using simple one-dimensional (1D) models,[3] and later they were observed in the laboratory.[4] The experimental observation of the BO was achieved due to the ability of grown high quality semiconductor superlattices.[5] The most important ingredient to explain WSL is the wavelike behavior of the electrons. Therefore, these ladders must also be observed in all classical undulatory systems. The existence of BO has been demonstrated in plenty of systems described by a wave equation. For instance, BO has been reported in ultracold atoms,[6,7] Bose-Einstein condensates,[8] light waves in photonic crystals,[9–11] and more recently in sound waves in phononic crystals,[12–15] proposing alternative ways to mimic the effects of the periodic potentials under external fields.

The photonic analog of BO has been widely studied and they appear when a photonic crystal is subjected to a slowly varying refractive index or a geometric parameter modulation, resulting in a linear tilting of the band structure. In the same way, it is possible to achieve this tilting of the acoustic band structure in phononic crystals. Different methods have been proposed to tilt the phononic band to observe the WSL and the corresponding acoustic Bloch Oscillations (ABOs). Recently, was predicted the existence of GHz-THz nanophononic BO and WSL in systems formed by a series of coupled acoustic nanocavities with lattice parameter changing linearly along the structure as a function of the position[16–18] and experimentally observed in samples of AlAs/GaAs grown by molecular beam epitaxy.[19] Surface acoustic waves in perturbed grating structures on a solid substrate and a layered structure consisting of alternate plane-parallel glass and water layers were used to study BO in the MHz range.[20,21] However, porous silicon (PS) is fabricated by an easier technique and provides good flexibility in the design of acoustical devices due to its tunable acoustic properties which allow us to design systems working in the GHz range.[22] PS can be obtained by electrochemical etching of doped silicon wafers, which allows the fabrication of several types of 1D porous silicon phononic bandgap structures such as distributed Bragg reflectors, microcavities,[23] and rugate filters.[24]

In the present work, we demonstrate the theoretical and experimental evidence of WSL in multilayer structures based on porous silicon, with a linear gradient in the η parameter. Theoretical results of the ABO in such structures are also presented. First, we designed a periodic structure formed by two kind of layers, *a* and *b*, tuning the second band gap around 1.1 GHz using an impedance mismatch as large as possible, in order to obtain the widest band-gap. Then we applied a gradient in the η parameter of layer *a*, keeping it constant for the layer *b*. Using this procedure, we get

a)Electronic address: arriaga@ifuap.buap.mx

localized modes corresponding to WSL, which are confirmed by our experimental measurements of the acoustic transmittance. From these experimental results, we calculate the evolution of a Gaussian pulse through the structures to observe the ABO. We obtain an excellent agreement with the results obtained theoretically.

II. THEORETICAL MODEL

In a solid, the acoustic waves can be either longitudinal or transversal. In this paper, we only consider longitudinal waves propagating through the PS. The propagation of longitudinal acoustic phonons in a one-dimensional (1D) layered structure is described by the wave equation

$$\rho_j \frac{\partial^2 u_j(z,t)}{\partial t^2} = (\lambda + 2\mu)_j \frac{\partial^2 u_j(z,t)}{\partial z^2}, \tag{1}$$

where ρ_j is the mass density, $(\lambda + 2\mu)_j = \rho v_{Lj}^2$ and $u(z, t)$ is the atomic displacement. Here, j is an index identifying each layer. The mass density ρ_j is a function of the porosity and is described by $\rho_j = \rho_0(1 - P_j)$, where $\rho_0 = 2.330\, g/cm^3$ is the mass density of bulk silicon and P_j is the porosity in the j-th layer. The acoustic velocity dependence on porosity is given empirically by[25,26]

$$v_L = v_{L0}(1 - P)^k, \tag{2}$$

where v_{L0} is the longitudinal velocity of sound in bulk silicon along the (100) crystallographic direction and $k \geq 0.5$ is a constant. In general, the parameter k depends on PS morphology which in turn depends on the doping level of the Si substrate.[22] We calculated v_{L0} and the parameter k for our samples, as is described later.

In each layer, lets say j, the solution of Eq. (1) takes the form

$$u(z_j, t) = [A_j^+ \exp(ik_j z_j) + A_j^- \exp(-ik_j z_j)]\exp(-i\omega t), \tag{3}$$

corresponding to waves propagating to the right (A^+) and left (A^-). At each interface, this solution must satisfy the boundary conditions related to the continuity of the atomic displacement and stress, i.e.,

$$u_j(d_j) = u_{j+1}(d_j) \tag{4}$$

and

$$\rho_j v_{Lj}^2 \frac{\partial u_j(d_j)}{\partial z}\bigg|_{z=d_j} = \rho_{j+1} v_{L(j+1)}^2 \frac{\partial u_{j+1}(d_j)}{\partial z}\bigg|_{z=d_j}, \tag{5}$$

respectively. Here, d_j denotes the position of the j-th interface between the j and $j + 1$ layers. The frequency ω of the acoustic wave is related to the wave vector via $\omega = v_j k_j$, where v_j is the speed of sound in the j-th layer and $\omega = 2\pi f$, with f being the frequency in s^{-1}. Using the matrix method,[27] we can relate the amplitudes of the waves A_j^+ (traveling to the right) and A_j^- (traveling to the left) in the j-th layer of the system with the amplitudes of the waves in the $j + 1$-th layer according to

$$\begin{pmatrix} A_j^+ \\ A_j^- \end{pmatrix} = T_j \begin{pmatrix} A_{j+1}^+ \\ A_{j+1}^- \end{pmatrix}. \tag{6}$$

The transfer matrix T_j appearing in the previous equation propagates the amplitudes through a layer with thickness d_j, mass density ρ_j, and sound longitudinal velocity v_{Lj}, and is given explicitly by

$$T_j = \begin{pmatrix} \cos(k_j d_j) & -i\sin(k_j d_j)/k_j v_{Lj}^2 \rho_j \\ -ik_j v_{Lj}^2 \rho_j \sin(k_j d_j) & \cos(k_j d_j) \end{pmatrix}. \tag{7}$$

If we consider a structure formed by N layers, the total transfer matrix representing the structure is obtained multiplying, in the appropriate order, a series of N transfer matrices, each one given by a matrix of the type appearing in Eq. (7). The obtained matrix relates the displacement vector at the beginning of the structure with that at the end and represents a 2×2 set of equations that can be fully solved.

With the above formalism, one can derive the acoustic eigenenergies and eigenvectors. The reflectivity and transmission spectrum of the structure can also be calculated as the square modulus of A_0^- and A_N^+, respectively, by imposing as boundary conditions $A_0^+ = 1$ and $A_N^- = 0$. Here, 0 and N label the first and last layers of the structure, respectively.

WSLs are observed in transmission spectrum (in frequency domain) and they appear as a series of peaks for given frequencies corresponding to the propagating modes along the system. However, to demonstrate the ABO in the time domain, we consider the propagation of a Gaussian pulse through the structure. The Gaussian pulse is described by $g(f) = \exp(-4\pi[(f - f_0)/\sigma]^2$, where f_0 is the central frequency and σ is the pulse width. In response to the incident pulse, the time and spatial variations of the displacement field $u(z, t)$ inside the sample can be calculated according to the scattering state method as[28]

$$u(z,t) = \frac{1}{2\pi}\int_{-\infty}^{+\infty} u(z,f)g(f)e^{-i2\pi ft} df, \tag{8}$$

where $u(z, f)$ is the displacement field distribution for each frequency, which is obtained by the transfer matrix method.

Because it is difficult to measure the field distribution inside the sample (it says nothing about the temporal field distribution), it is hard to experimentally demonstrate the ABO in the same way as in the simulation. However, since the ABO inside the sample affects the time dependent transmission spectra, the ABO can be alternatively demonstrated by this way. Because we have results in the frequency domain only, we can use the scattering state method to obtain the time dependence from the frequency domain of the transmission coefficient. The time dependence transmission coefficient can be obtained from

$$T(t) = \frac{1}{2\pi}\int_{-\infty}^{+\infty} T(f)g(f)e^{-i2\pi ft} df, \tag{9}$$

where $T(f)$ is the experimentally determined transmission coefficient as a function of frequency f. This equation is

formally equivalent to the Fast Fourier Transform (FFT) method used below to determine the acoustic longitudinal velocity, but it includes Gaussian windowing. In the experiments, this windowing is done by the transducers response, which has Gaussian like shape.

Here, we present calculations and measurements of acoustic transmission and time evolution of Gaussian pulses in both, theoretical and experimental results, as well as calculations of the displacement distribution, and time evolution of acoustic pulses inside the sample to demonstrate the existence of acoustic Wannier-Stark ladders and acoustic Bloch oscillations.

III. EXPERIMENTAL DETAILS

Single-layer and multilayer porous structures were electrochemically etched from boron-doped (100)-oriented Si substrates with a resistivity of 0.007–0.013 Ω·cm. Room-temperature anodization was performed using a 1:1 solution of HF (40%) and ethanol (99.98%). Single PS layers of thicknesses in the range of 60–100 μm and porosities in the range of 42%–73% were prepared in order to measure the longitudinal velocity as a function of porosity. The layers were etched at these thicknesses to give a resolvable time-of-flight for sound waves in the porous layer.[29] The acoustic transmission measurements reported here were done using a Vector Network Analyzer (VNA). Each sample was placed between two ZnO-based piezoelectric transducers with a central frequency of 1.1 GHz and an operation bandwidth of ~500 MHz. The transducers consist of a piezoelectric layer driving waves into a silicon pillar with thickness of 500 μm. To couple the transducers to the specimen, deionized water was used. The transducer front surface was aligned parallel to the sample surface using two orthogonal microscopes, so that the acoustic waves impinge normally into the PS layers. The transducers were connected to the VNA ports and transmission parameters were measured as function of frequency.

To measure the sound velocity, analysis of the transmitted signal was done using the equivalent response in time domain, which was calculated using a FFT algorithm incorporating both the amplitude and phase. With the frequency sampling employed, we have a resolution of ~2 ns. The transmitted signal through a single porous monolayer attached to the silicon substrate appears in Figure 1(a). Each peak appearing in this spectrum can be identified if we consider all the components in the experimental setup. The first and strongest peak corresponds to the directly transmitted signal arriving at a time t1 of ~195 ns (Figure 1(b)). The other peaks appearing in the spectra are delayed respect to the first peak, and they are associated to one or more roundtrips in the coupling water (t_2), sample (t_3, t'_3, t''_3), substrate (t_4), or transducer (t_5) layers. Figure 1(a) shows the transmitted signal amplitude in time domain and the peaks associated with roundtrips in PS and Si layers and labeled accordingly to the scheme shown at the right part of the figure. Thicknesses, d (PS layer) and D (substrate), were measured by optical microscopy, and the porosities were determined by analysis of the Fabry-Perot interference fringes from optical reflectance spectra by fitting our experimental measurements and comparing them with our theoretical simulations for each sample.

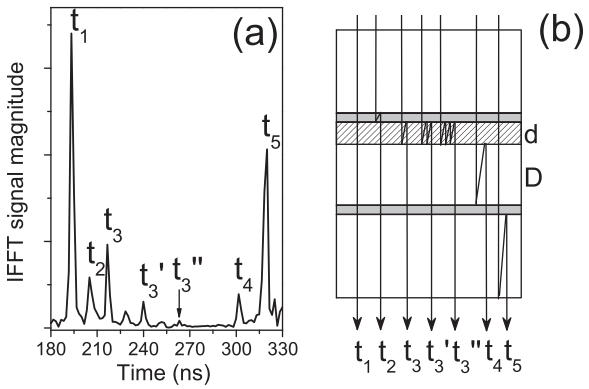

FIG. 1. Transmitted signal amplitude in time domain and schematic illustration of the different reflection paths in the layers forming the system.

The longitudinal velocity for the PS layer can be easily calculated as (see Figure 1(b))

$$v_L = \frac{2d}{t_3 - t_1} = \frac{4d}{t'_3 - t_1} = \frac{6d}{t''_3 - t_1} \tag{10}$$

and, simultaneously, the longitudinal velocity for the bulk silicon substrate v_{L0} can be also calculated from

$$v_{L0} = \frac{2D}{t_4 - t_1}. \tag{11}$$

In Figure 2, we show the measured and calculated velocities for both porous silicon samples with different porosities and the attached part of the silicon remaining in the wafer. The squares (circles) correspond to the longitudinal velocity for PS (silicon) layers determined from Eq. (10) (11) using the measured times. The dashed line is the average value ($v_{L0} = 8.44$ km/s) obtained from our experimental results. This value agrees with the reported value for the velocity of [100] longitudinal waves in crystalline silicon.[26,30] If we fit the porosity data and the determined velocity ($v_{L0} = 8.44 \pm 0.02$ km/s), to the semi-empirical formula given by Eq. (2), we found $k = 0.560 \pm 0.015$. The solid line in Figure 2 corresponds to this fitting. Our results

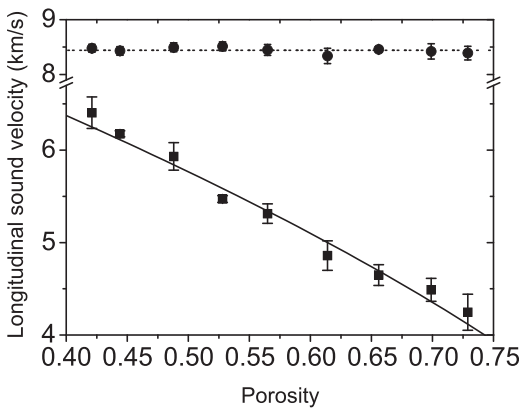

FIG. 2. Experimental values of longitudinal velocity for PS single layers as a function of porosity. Theoretical fit for $v_L = v_{L0}(1-p)^k$, $k = 0.56$ (solid line), and $v_{L0} = 8.44$ km/s (dashed line) corresponding to the average of experimental values for Si substrate.

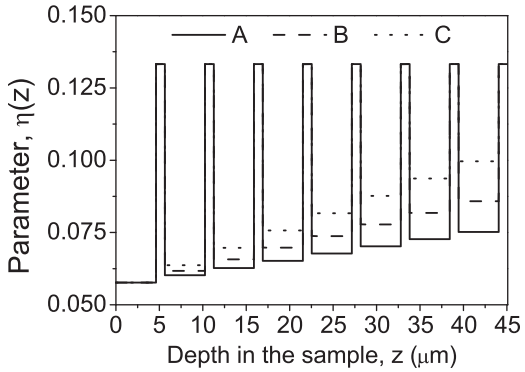

FIG. 3. Profile of parameter η as a function of the depth in the structures: A (solid line), B (dashed line), and C (dotted line).

agree with those reported before using similar samples and etching conditions.[30]

To demonstrate acoustic WSL (AWSL), we have considered three different structures, each one with a different linear gradient on the $\eta(z)$ parameter along the growth direction. This parameter is the equivalent to the dielectric constant in optics. In the acoustic case $\eta(z) = 1/v_L^2(z)$, where $v_L(z)$ is the longitudinal sound velocity at z.[31] We fabricated three different samples, obtained repeating periodically two layers a and b with different porosity, and denoted as A, B, and C. The number of periods considered must be large enough to obtain well defined acoustics gaps. In the three samples, layer b has a constant porosity of 73% and thickness $d_b = 1.01$ μm; meanwhile the porosity in layer a, with thickness $d_a = 4.62$ μm in the three samples, varies gradually along the growth direction. The linear gradient introduced in layer a corresponds to porosities variation from 43% to 55%, from 43% to 60%, and from 43% to 65% for the samples A, B, and C, respectively. The porosities and thicknesses of the layers were chosen in order to obtain the first acoustic stop band within the bandwidth of the acoustic transducers used for transmittance measurements, i.e., between 0.5 and 1.5 GHz. A schematic representation of the η parameter as a function of the depth in the structures A, B, and C is shown in Figure 3.

For the fabrication of PS multilayers, we consider the inclusion of "etch stops" or "etch breaks" where the current is interrupted to stop the etching of the Si wafer in order to prevent the depletion of HF. The introduction of these etching breaks is necessary to obtain layers with constant porosity with depth.[32] Since our samples include very thick layers, with large mismatch porosities between them, the number and length of the etch breaks are important to obtain homogeneous structures. We found that etch breaks of 6 s with a ratio (etch break time)/(etching time) from 2 for low porosities to 14 for high porosities are enough to minimize any chirp in the layers.

IV. RESULTS AND DISCUSSION

The acoustic transmission and field intensity distribution have been modeled using the transfer matrix method described before and taking into account the effect of the sample (PS-Si substrate), transducers (Si pillars), and In-Ga eutectic liquid used to couple the transducers to the sample. In Figure 4, we show the theoretical transmission spectra for the samples considered here. The linear gradient imposed over the η parameter in the structure leads to a sequence of localized frequency levels, i.e., the expected AWSL. These levels are clearly observed in Figures 4(a)–4(c). In Figures 4(d)–4(f), we show the field displacement distribution as a function of position and frequency for acoustic waves impinging from the left on the structures. Brighter narrow horizontal lines correspond to larger acoustic field intensities and they are the proper modes of the tailored acoustic structure corresponding to the AWSL. The spacing between levels, Δf, depends on the tilt of the band structure. For the sample A, which has the smaller tilt, the spacing between levels obtained is ~43 MHz. For sample B, this level spacing is $\Delta f \sim 46$ MHz; meanwhile for the structure C, the spacing level obtained is $\Delta f \sim 50$ MHz.

The WSL is the spectral domain counterpart of the BO. A system having such a discrete sequence of frequency levels with level spacing f is the acoustical equivalent of the electronic WSL and is expected to exhibit ABO of period $\tau_B = 1/\Delta f$. In Figures 4(g)–4(i), we show the time resolved transmission $T(t)$, corresponding to the time evolution of a Gaussian pulse in the samples calculated using Eq. (9). Values of 1.197 GHz, 1.157 GHz, and 1.113 GHz were used for the central frequency f_0 of the Gaussian pulse for the structures A, B, and C, respectively. These values correspond to the frequencies where the AWSL appear. From Figures 4(g)–4(i), we can clearly observe the oscillatory behaviour of the transmission spectra. The transmission spectra oscillate in time with constant period τ. The period of the ABO (τ_B) obtained from these figures are: ~23.5 ns for structure A, ~21.7 ns for B, and ~19.9 ns for structure C. The period of the ABO obtained from the spacing between levels of AWSL using $1/\Delta f$ is: 23.25 ns, 21.73 ns, and 20 ns for the structures A, B, and C, respectively. Of course, different tilts lead to different Bloch periods.

Experimental measurements of the acoustic transmission, using the experimental set-up described before, are shown in Figure 5. We can see that AWSL appear as localized modes in transmission spectrum for the three samples. Apart from a small blue-shit, there is an excellent agreement between the theoretical (Figs. 4(a)–4(c)) and the experimental results.

To probe the presence of ABO, we calculated the time evolution of a Gaussian pulse in each sample as defined in Eq. (9), substituting the experimental measurements of $T(f)$. This procedure allows us to obtain the time evolution of the transmission spectrum, $T(t)$, from the experimental values of $T(f)$. Time-resolved transmission spectra of the samples, with more oscillating cycles, are presented in Figure 6. From this figure, we can clearly observe the acoustic Bloch oscillations: The transmission spectrum oscillates in time with a constant period τ_B. Values for f_0 of 1.260, 1.157, and 1.055 GHz were used for samples A, B, and C, respectively, and $\sigma = 200$ MHz for all samples. We have considered different values of the pulse width σ, and we observed that the obtained results are not sensitive to the value of this parameter. The role of the parameter

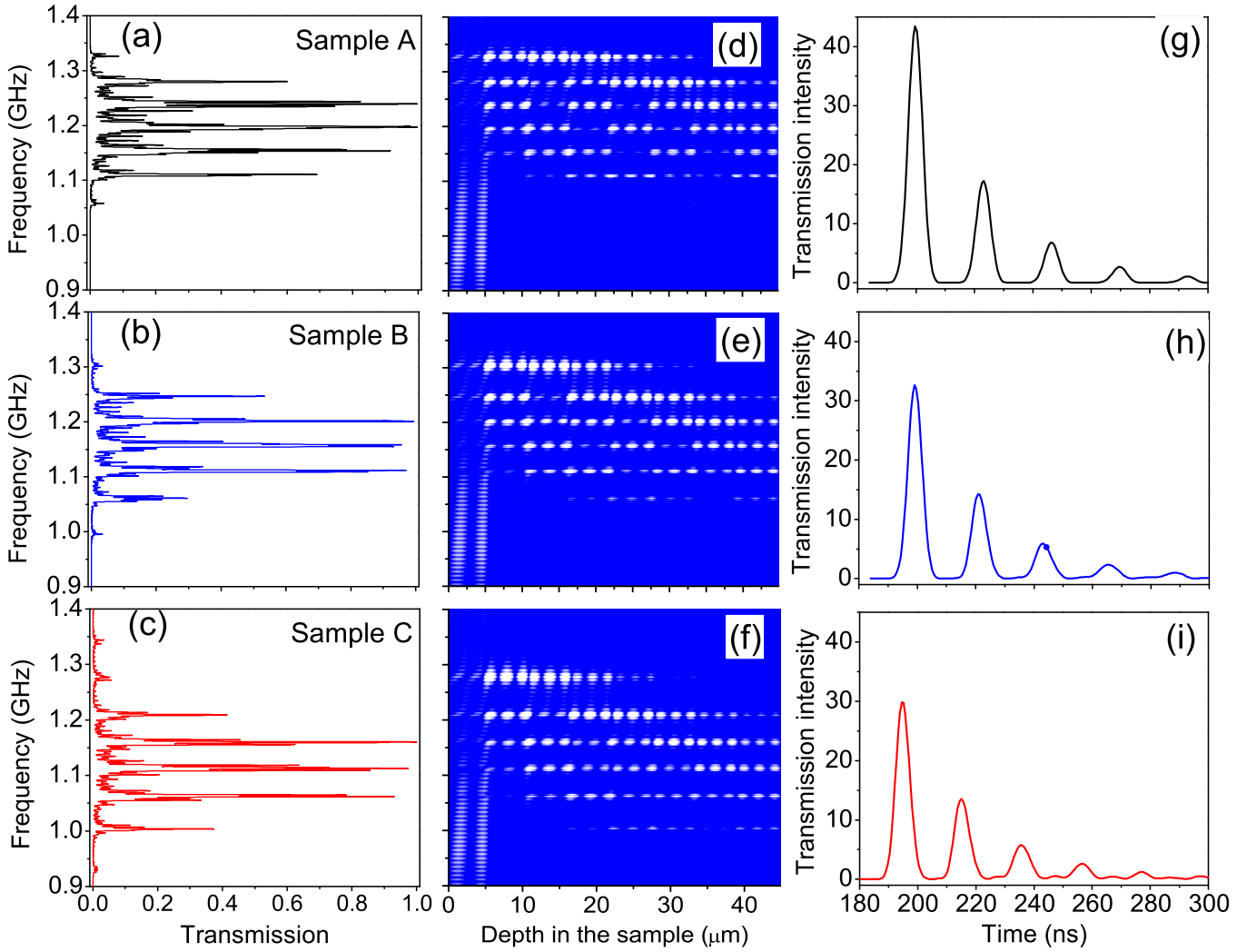

FIG. 4. Transfer matrix calculations for transmission ((a)–(c)), field displacement distribution as a function of position and frequency ((d)–(f)), and time resolved transmission spectra ((g)–(i)) for the structures considered here: A, B, and C.

σ is to window the interval of frequency we are testing. The oscillation period of the ABO obtained from the experimental measurements are: ~27 ns for sample A, ~24 ns for sample B, and ~19 ns for samples C; against 23.5, 21.7, and 19.9 ns, the values obtained from the theoretical simulations. It can be clearly seen that the value of the period oscillation, τ_B, decreases when the tilt increases, and this is because the mini-band tilt gets steeper.

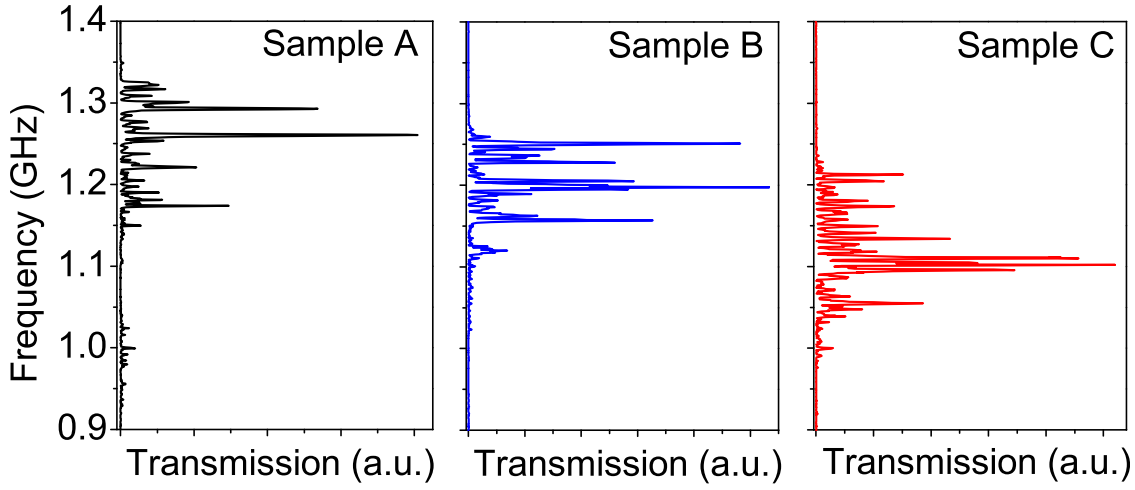

FIG. 5. Measured acoustic transmission for samples A, B, and C, from left to right.

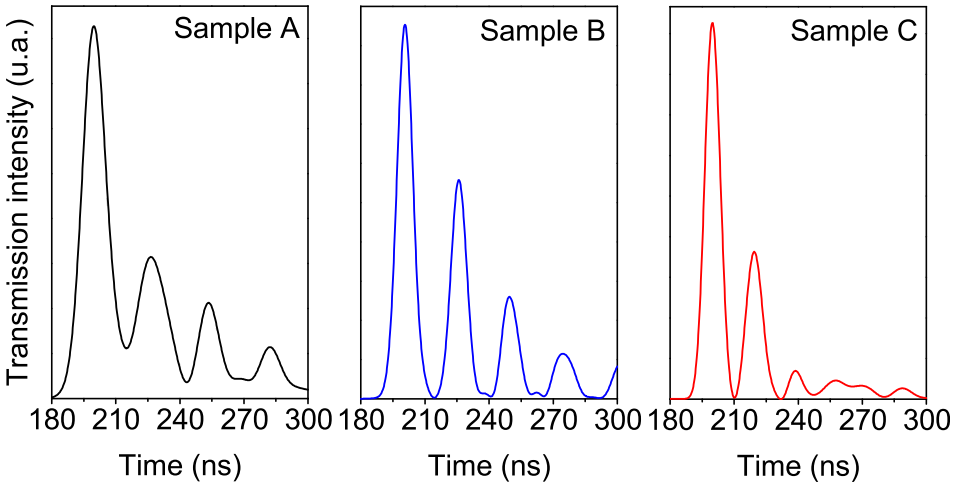

FIG. 6. Time resolved transmission spectrum calculated from the experimental measurements using a Gaussian pulse traveling through the samples.

V. CONCLUSIONS

AWSL and ABO were theoretically calculated and successfully measured experimentally in PS multilayer structures based on PS. The considered structures include a linear gradient in the η parameter to emulate a periodic potential under an external field. By introducing this linear gradient, we observed the AWSL in the acoustic transmission spectra. By changing this gradient, we tune the period of the ABO in PS structures. This allows us to control the acoustic waves, which is important in designing acoustic devices.

ACKNOWLEDGMENTS

This work has been partially supported by CONACyT under Project No. 167939.

[1]F. Bloch, Z. Phys. **52**, 555 (1929); C. Zener, Proc. R. Soc., London, Ser. A **145**, 523 (1934).
[2]G. H. Wannier, Phys. Rev. **117**, 432 (1960).
[3]S. Nagai and J. Kondo, J. Phys. Soc. Jpn. **49**, 1255 (1980).
[4]E. E. Méndez, F. Agulló-Rueda, and J. M. Hong, Phys. Rev. Lett. **60**, 2426 (1988); J. Bleuse, G. Bastard, and P. Voisin, *ibid.* **60**, 220 (1988).
[5]J. Feldmann, K. Leo, J. Shah, D. A. B. Miller, J.-E. Cunningham, T. Meier, G. von Plessen, A. Schulze, P. Thomas, and S. Schmitt-Rink, Phys. Rev. B **46**, 7252 (1992); K. Leo, P. H. Bolivar, F. Brüggemann, R. Schwedler, and K. Köhler, Solid State Commun. **84**, 943 (1992); T. Dekorsy, P. Leisching, K. Köhler, and H. Kurz, Phys. Rev. B **50**, 8106 (1994).
[6]C. Waschke, H. G. Roskos, R. Schwedler, K. Leo, H. Kurz, and K. Köhler, Phys. Rev. Lett. **70**, 3319 (1993).
[7]M. BenDahan, E. Peik, J. Reichel, Y. Castin, and C. Salomon, Phys. Rev. Lett. **76**, 4508 (1996).
[8]B. P. Anderson and M. A. Kasevich, Science **282**, 1686 (1998).
[9]V. Agarwal, J. A. del Río, G. Malpuech, M. Zamfirescu, A. Kavokin, D. Coquillat, D. Scalbert, M. Vladimirova, and B. Gil, Phys. Rev. Lett. **92**, 097401 (2004).
[10]R. Morandotti, U. Peschel, J. S. Aitchison, H. S. Eisenberg, and Y. Silberberg, Phys. Rev. Lett. **83**, 4756 (1999).
[11]R. Sapienza, P. Costantino, D. Wiersma, M. Ghulinyan, C. J. Oton, and L. Pavesi, Phys. Rev. Lett. **91**, 263902 (2003).
[12]N. D. Lanzillotti Kimura, A. Fainstein, and B. Jusserand, Phys. Rev. B **71**, 041305(R) (2005).
[13]H. Sanchis-Alepuz, Yu. A. Kosevich, and J. Sanchez-Dehesa, Phys. Rev. Lett. **98**, 134301 (2007).
[14]Z. He, S. Peng, F. Cai, M. Ke, and Z. Liu, Phys. Rev. E **76**, 056605 (2007).
[15]L. Gutierrez, A. Díaz-de-Anda, J. Flores, R. A. Meéndez-Sánchez, G. Monsivais, and A. Morales, Phys. Rev. Lett. **97**, 114301 (2006).
[16]N. D. Lanzillotti Kimura, A. Fainstein, C. A. Balseiro, and B. Jusserand, Phys. Rev. B **75**, 024301 (2007).
[17]M. Trigo, A. Bruchhausen, A. Fainstein, B. Jusserand, and V. Thierry-Mieg, Phys. Rev. Lett. **89**, 227402 (2002).
[18]P. Lacharmoise, A. Fainstein, B. Jusserand, and V. Thierry-Mieg, Appl. Phys. Lett. **84**, 3274 (2004).
[19]N. D. Lanzillotti-Kimura, A. Fainstein, B. Perrin, B. Jusserand, O. Mauguin, L. Largeau, and A. Lemaitre, Phys. Rev. Lett. **104**, 197402 (2010).
[20]M. M. de Lima, Yu. A. Kosevich, P. V. Santos, and A. Cantarero, Phys. Rev. Lett. **104**, 165502 (2010).
[21]A. A. Karabutov, Yu. A. Kosevich, and O. A. Sapozhnikov, Acoust. Phys. **59**, 137 (2013).
[22]G. N. Aliev, B. Goller, and P. A. Snow, J. Appl. Phys. **110**, 043534 (2011).
[23]G. N. Aliev, B. Goller, D. Kovalev, and P. A. Snow, Appl. Phys. Lett. **96**, 124101 (2010).
[24]L. Thomas, G. N. Aliev, and P. A. Snow, Appl. Phys. Lett. **97**, 173503 (2010).
[25]K. K. Phani, S. K. Niyogi, A. K. Maitra, and M. Roychaudhury, J. Mater. Sci. **21**, 4335 (1986); A. K. Maitra and K. K. Phani, *ibid.* **29**, 4415 (1994).
[26]R. J. M. Da Fonseca, J. M. Saurel, A. Foucaran, J. Camassel, E. Massone, T. Taliercio, and Y. Boumaiza, J. Mater. Sci. **30**, 35 (1995); R. J. M. Da Fonseca, J. M. Saurel, A. Foucaran, E. Massone, T. Taliercio, and J. Camassel, Thin Solid Films **255**, 155 (1995).
[27]C. L. Mitsas and D. I. Siapkas, Appl. Opt. **34**, 1678 (1995).
[28]G. Malpuech, A. Kavokin, G. Panzarini, and A. Di Carlo, Phys. Rev. B **63**, 035108 (2001).
[29]Z. Lazcano and J. Arriaga, Prog. Electromagn. Res. **1**, 1404 (2013).
[30]G. N. Aliev, B. Goller, D. Kovalev, and P. A. Snow, Phys. Status Solidi C **6**, 1670–1674 (2009).
[31]G. Monsivais, M. del Castillo-Mussot, and F. Claro, Phys. Rev. Lett. **64**, 1433 (1990).
[32]M. Thönissen, M. G. Berger, S. Billat, R. Arens-Fischer, M. Krüger, H. Lüth, W. Theiss, S. Hillbrich, P. Grosse, G. Lerondel, and U. Frotscher, Thin Solid Films **297**, 92 (1997).